Available online at www.sciencedirect.com
ScienceDirect
Polymer 48 (2007) 7660–7671
polymer
www.elsevier.com/locate/polymer

Formation of phase structure and crystallization behavior in blends containing polystyrene–polyethylene block copolymers

Hiroki Takeshita, Yuan-Ji Gao, Tomoyuki Natsui, Erick Rodriguez, Masamitsu Miya, Katsuhiko Takenaka, Tomoo Shiomi*

Department of Materials Science and Technology, Nagaoka University of Technology, 1603-1 Kamitomioka, Nagaoka, Niigata 940-2188, Japan

Received 9 August 2007; received in revised form 17 October 2007; accepted 3 November 2007
Available online 7 November 2007

Abstract

The microphase separation structure in the molten state and the structure formation in crystallization from such ordered melt were investigated for the blends of polystyrene–polyethylene block copolymers (SE) with polystyrene homopolymer (PS) and polyethylene homopolymer (PE) and for the blends consisting of two kinds of SE with different copolymer compositions from each other, using synchrotron small-angle X-ray scattering techniques (SAXS). The copolymer compositions of SE block copolymers employed were 0.34, 0.58 and 0.73 wt. fraction of PE, and their melt morphologies were cylindrical, lamellar and lamellar, respectively. Macrophase separation or the morphology change in the melt occurred depending on the molecular weight and the blend composition, as reported so far. In crystallization from such macrophase-separated and microphase-separated melts, the melt morphology was completely kept for all the blends. Crystallization behavior was also investigated for the blends. The crystallization within the spherical and cylindrical domains surrounded by glassy PS was not observed for SE/PS blends. In the crystallization from the macrophase-separated melt, two exothermal peaks were observed in the DSC measurements, while a single peak was observed for other blends. For the blends with PS, the degree of crystallinity was depressed and the apparent activation energy of crystallization was high, compared to those for the corresponding neat SE. For SE/PE and SE/SE blends, those were changed depending on the blend composition.

Keywords: Crystallization; Microphase separation; Polystyrene–polyethylene block copolymer

1. Introduction

Crystallization and higher-order structure formation of crystalline–amorphous block copolymers have been extensively studied [1–18]. In crystallization at a temperature below the order–disorder transition temperature T_{ODT}, it is of main interest whether or not microphase separation structure in the melt is destroyed by crystallization, that is, whether block copolymers crystallize within a microdomain or not. When the amorphous block is in the rubbery state at a crystallization temperature T_c of the crystalline block, the structure change in crystallization is governed by kinetic factors such as competition between crystallization rate and diffusion rate of the amorphous chain, because polymers are usually made to crystallize in the state far from the equilibrium state. We have elucidated that structure change in crystallization depends on the melt morphology as well as the crystallization temperature [16]. When the amorphous block is in the glassy state, on the other hand, it is expected that microphase separation structure in the melt will be preserved in crystallization because the amorphous domain remains rigid throughout the crystallization process [18].

We reported the crystallization and structure formation of di- and tri-block copolymers consisting of polyethylene (PE) and polystyrene (PS) [18]. In this article, further studies, which are concentrated on the blends of PE–PS block copolymers with the corresponding homopolymers, PE and PS, and on the blends consisting of two kinds of PE–PS block copolymers, are presented. In the blends containing block copolymers, the melt morphology and the domain size may be changed and the macrophase separation may also occur depending on the blend ratio. This article is focused on the crystallization from such phase structure in the melt.

* Corresponding author. Tel.: +81 258 47 9304; fax: +81 258 47 9300.
E-mail address: shiomi@vos.nagaokaut.ac.jp (T. Shiomi).

0032-3861/$ - see front matter © 2007 Elsevier Ltd. All rights reserved.
doi:10.1016/j.polymer.2007.11.002

2. Experimental section

2.1. Materials

Polystyrene–polyethylene block copolymers (SE) and polyethylene homopolymers (PE) were synthesized by catalytic hydrogenation of the corresponding precursor polystyrene-polybutadiene block copolymers (SB) and polybutadiene homopolymers (PBd), respectively, purchased from Polymer Source, Inc. Hydrogenation was carried out in degassed toluene (1–1.5 wt% solution of the block copolymer) at 90 °C and 6 MPa H_2 pressure for 30 h using a Wilkinson catalyst $(Ph_3P_3)_3Rh(I)Cl/(C_6H_5)_3P$ (1.0 mol%/35 mol% with respect to the number of double bonds of the PBd blocks, respectively). Purification was accomplished by repeated precipitation with a toluene/methanol system three times and dried under vacuum for a day. Under the used conditions, the PBd blocks got completely hydrogenated and the PS blocks were not hydrogenated as revealed by 400-MHz ^{1}H NMR. Gel permeation chlomatography (GPC) traces for all hydrogenated polymers indicated a narrow single peak which was almost the same as that in the original PBd polymers. The ratio of 1,2-structure to 1,4-structure estimated for the original butadiene polymers with ^{1}H NMR was 7/93 or 8/92(mol/mol), which corresponds to 3.5 or 4.0%, respectively, of ethyl branches per ethylene unit for polyethylene. Characteristics of the samples employed are listed in Table 1.

Table 1
Characteristics of SE block copolymers and PE, PS homopolymers

Sample	Sample code	M_w/M_n[a]	M_n[b] [kg/mol]		Composition (wt%)		Branch[c] (1-butene, mol%)
			PS	PE	PS	PE	
SE	SE34	1.03	28.4	14.1	66	34	3.5
	SE54	1.05	36.9	42.4	46	54	4.0
	SE73	1.04	15.4	40.0	27	73	3.5
PE	HPE	1.05	–	40.0	–	100	4.0
	LPE	1.02	–	6.5	–	100	4.0
PS	HPS	1.02	9.5	–	100	–	–
	LPS	1.03	5.6	–	100	–	–

[a] Determined by SEC in toluene calibrated against polystyrene standards.
[b] Nominal value in which hydrogenation was taken into account of.
[c] Determined by ^{1}H NMR spectroscopy in C_6D_6.

2.2. Sample preparation and measurements

The block copolymers and blends were cast from a 5 wt% solution in toluene at 60 °C, followed by removing the solvent completely in a vacuum oven at room temperature for 1 day. The compositions of the blends used are shown in Table 2.

Table 2
Spacing, domain size and morphology estimated from SAXS

Sample	Composition (wt%)		Composition of PE (wt%)	Spacing L (nm)	Domain size[a]		Morphology in the melt
	Block	Homo			d_{PS}(nm)	d_{PE} (nm)	
SE34	100	0	34	43.5	–	16.7[b]	PE cylinder
SE54	100	0	54	79.3	31.2	48.1	Lamella
SE73	100	0	73	59.1	14.5	44.6	Lamella
HPE	0	100	100	36.0[c]	–	–	–
LPE	0	100	100	17.0[c]	–	–	–
SE54/HPS-43	80	20	43	87.7	43.9	43.8	Lamella
SE54/LPS-43	80	20	43	83.3	41.7	41.6	Lamella
SE54/HPS-27	50	50	27	109.6	–	38.2[b]	PE cylinder
SE54/LPS-27	50	50	27	102.0	–	35.6[b]	PE cylinder
SE73/HPS-52	71	29	52	95.0	–	44.2[b]	PE cylinder
SE73/LPS-52	71	29	52	83.8		39.0[b]	PE cylinder
SE73/HPS-26	36	64	26	–	–	–	PE sphere
SE73/LPS-26	36	64	26	–	–	–	PE sphere
SE34/HPE-58	64	36	58	75.8/49.7	–	–	Lamella/cylinder
SE34/LPE-58	64	36	58	79.9	28.4	51.5	Lamella
SE34/HPE-67	50	50	67	51.9/–	–	–	Cylinder/disorder
SE34/LPE-67	50	50	67	–	–	–	Lamella
SE54/HPE-63	80	20	63	–	–	–	Lamella
SE54/LPE-63	80	20	63	106.0	32.7	73.3	Lamella
SE54/HPE-82	40	60	82	–	–	–	Disorder?
SE54/LPE-82	40	60	82	–	–	–	Disorder?
SE54/SE34-41	33	67	41	61.9	32.3	29.6	Lamella
SE54/SE34-47	67	33	47	–	–	–	–
SE73/SE34-47	33	67	47	49.3	22.7	26.6	Lamella
SE73/SE34-60	67	33	60	55.8	18.7	37.1	Lamella
SE73/SE54-60	33	67	60	73.3	24.6	48.7	Lamella
SE73/SE54-67	67	33	67	67.4	18.3	49.1	Lamella

[a] Calculated using the specific volumes $v_{sp} = 1.283$ and 0.974 cm^3/g for amorphous PE [20] and PS [21], respectively, on the basis of the value of spacing L in melt.
[b] Radius of cylinder domain.
[c] Long period.

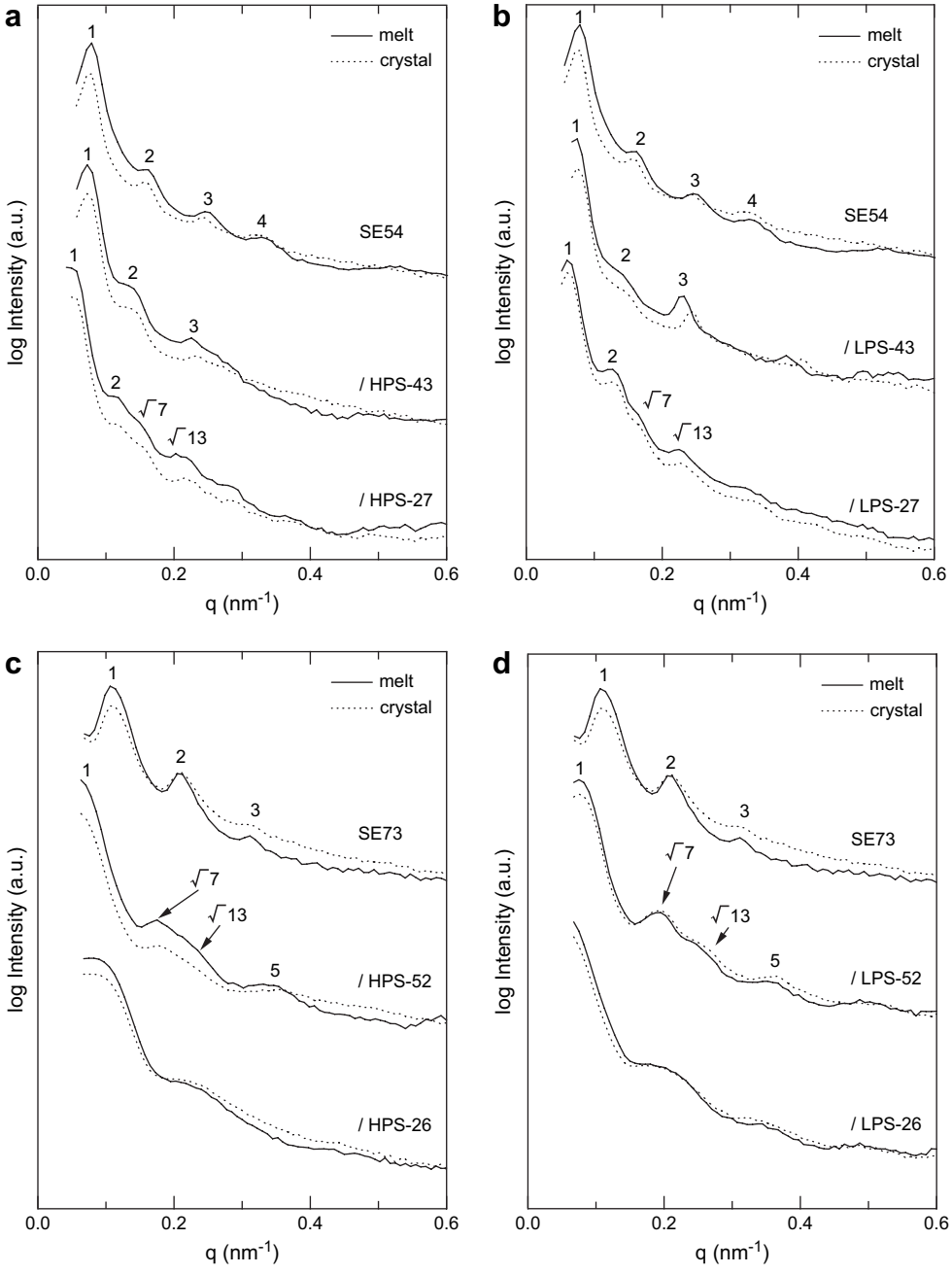

Fig. 1. SAXS profiles for SE and SE/PS in the molten state at 140 °C and the crystalline state at 74 °C.

Crystallization and melting processes were observed using time-resolved small-angle X-ray scattering technique employing synchrotron radiation (SR-SAXS). SR-SAXS measurements were performed with a beam line BL-10C at the Photon Factory in the Institute of Materials Structure Science, High Energy Accelerator Research Organization in Tsukuba, Japan. Details of the optics and the instrumentation have been described elsewhere [19]. The scattering vector was defined as $q = (4\pi/\lambda)\sin(\theta/2)$, where θ is the scattering angle.

The sample was annealed in a sample holder kept at 140 °C, which is higher than both melting temperature T_m of PE and glass-transition temperature T_g of PS, for 1 h to erase

Table 3
Characterization of microphase structure for SE/PS blends

Sample	D (nm)	D/D_0	a_y/a_{J0}
SE54	79.3	1	1
SE73	59.1	1	1
SE54/HPS-43	87.7	1.11	1.05
SE54/LPS-43	83.3	1.05	1.08
SE54/HPS-27	126.5	1.60	1.13
SE54/LPS-27	117.7	1.48	1.17
SE73/HPS-52	95.0	1.61	1.09
SE73/LPS-52	83.8	1.42	1.17

the previous thermal history and to form a stable microphase separation structure. Then, it was moved rapidly into a measurement holder thermostated at a desired crystallization temperature T_c to be crystallized isothermally.

Differential scanning calorimetry (DSC) measurements were performed with a Perkin–Elmer Pyris 1 apparatus. The sample was annealed at 140 °C for 30 min in the DSC apparatus, and then rapidly quenched to a desired T_c to be crystallized isothermally. Isothermal crystallization was analyzed by an exothermal peak. After the isothermal crystallization, melting behavior was observed by heating the sample from T_c to 140 °C at 5 °C/min.

3. Results and discussion

3.1. Microphase structure in molten and crystalline states

3.1.1. Blends with PS homopolymer

Fig. 1 shows SAXS profiles of SE and SE/PS in the molten and crystalline states.

In the molten state, for SE54 and its blends, microphase separation occurs for all samples, while macrophase separation does not appear to occur. This comes from the fact that the molecular weight of both LPS and HPS is smaller than

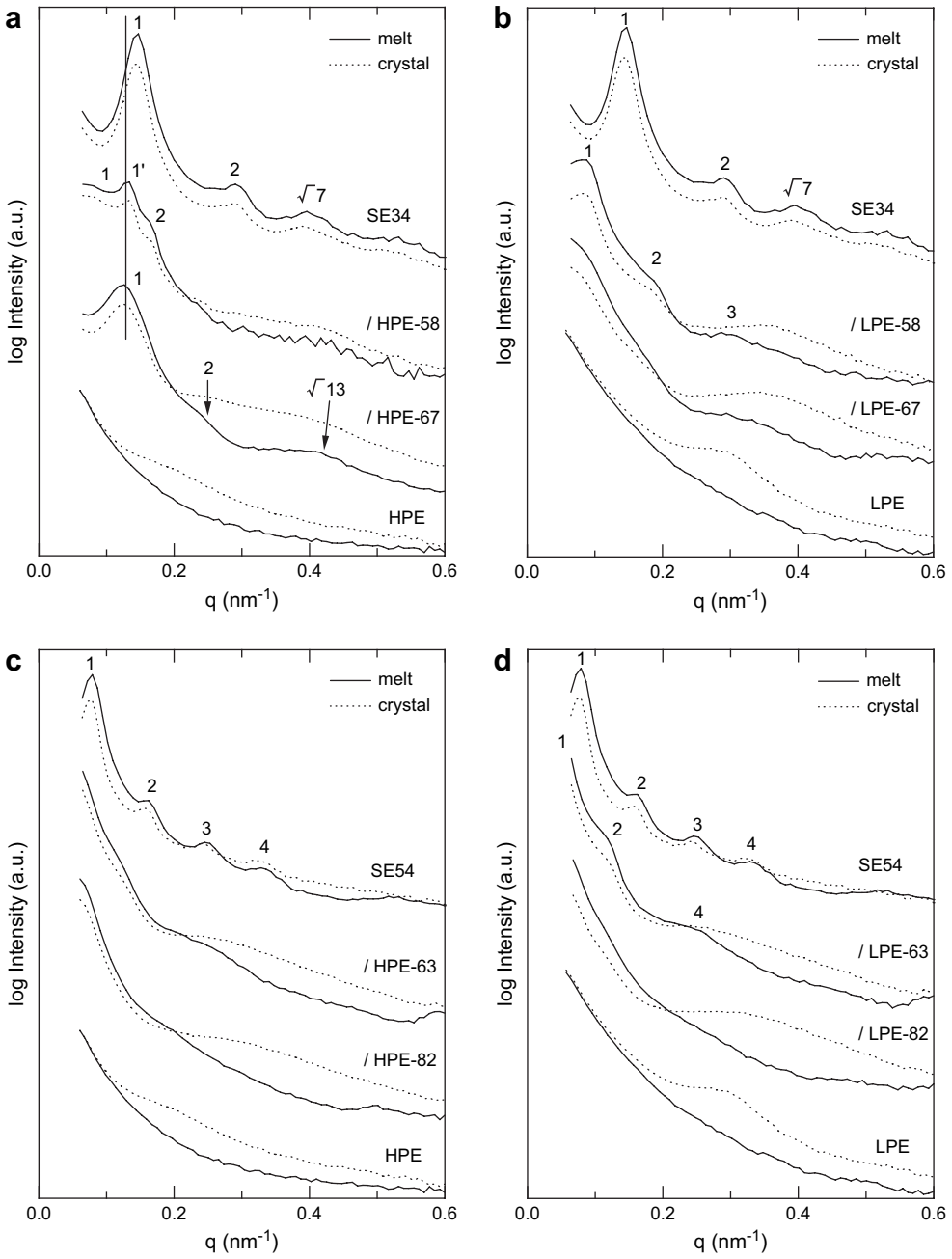

Fig. 2. SAXS profiles for SE and SE/PE in the molten state at 140 °C and the crystalline state at 74 °C.

that of the PS block of SE54 and that the amount of added PS is not so much. The microphase structure of the neat SE54 is maintained for SE54/HPS-43 and SE54/LPS-43 containing 20% of HPS and LPS, respectively, while for SE54/HPS-27 and SE54/LPS-27 containing 50% of PS homopolymer the microphase structure changed from lamella to cylinder.

The SE73 blends with PS homopolymer also show microphase separation structure. The morphology of SE73/LPS-52 and SE73/HPS-52 containing 29 wt% of PS homopolymer is a cylinder although the first-order peak for SE73/HPS-52 is hidden by the beam stopper. For SE73/LPS-26 and SE73/HPS-26 with more amount of PS, the SAXS peaks may come from particle scattering. This suggests that the spherical domains of PE are dispersed in the PS matrix.

The positions of the scattering peaks in these blends shift to smaller q from that in the respective neat block copolymers, which mean that the homopolymer is located in the microdomain. The spacing L estimated from the position of the first-order peak is summarized in Table 2. The domain sizes d of PS and PE evaluated from L using the volume fraction are also shown in Table 2, where the volume fraction was determined using the respective specific volumes, $v_{sp}(PE) = 1.283\ cm^3\ g^{-1}$ [20] and $v_{sp}(PS) = 0.974\ cm^3\ g^{-1}$ [21]. The interdomain distance D estimated for SE/PS blends is shown in Table 3. From the volumetric consideration it is possible to interrelate the ratio of D for the blend to D_0 for the neat block copolymer, with the change of the interfacial density ρ_J/ρ_{J0} of the chemical junctions, which is intimately related to the swelling of the solubilization behavior. Following Hashimoto et al. [22],

$$\frac{D}{D_0} = \left(\frac{\rho_J}{\rho_{J0}}\right)\phi_b^{-1} \tag{1}$$

for lamellar microdomains, and

$$\frac{D}{D_0} = \left(\frac{\rho_J}{\rho_{J0}}\right)\left[\left(2/3^{1/2}\right)\pi f \phi_b^{-1}\right]^{1/2} \tag{2}$$

for hexagonally packed cylindrical microdomains, where ϕ_b and f are the volume fraction of the block copolymer in the blend and the volume fraction of the desired component in the copolymer, respectively. ρ_J/ρ_{J0} can be related to a_J/a_{J0},

$$\left(\frac{\rho_J}{\rho_{J0}}\right) \approx \left(\frac{a_J}{a_{J0}}\right)^{-2} \tag{3}$$

where a_J/a_{J0} are the ratio of the average nearest-neighbor distance between the chemical junctions along the interface. When $a_J/a_{J0} = 1$, homopolymers are localized in the central regions of the domain, while homopolymers are more uniformly distributed in the domain as a_J/a_{J0} is larger. As compared between the blends with the same composition of HPS and LPS, namely, (SE54/HPS-43 and /LPS-43), (SE54/HPS-27 and /LPS-27), and (SE73/HPS-52 and /LPS-52), as shown in Table 3, D/D_0 for the HPS blends is larger than that for the LPS blends, and a_J/a_{J0} is smaller for the HPS blends than for the LPS blends. This means that PS homopolymer with a higher molecular weight is more localized in the central region of the domain.

At $T_c = 74\ °C$, as shown in the SAXS profiles drawn by the dotted line, the positions of the peaks including higher-order peaks are completely the same as those in the molten state. Here, note that any exothermal peak due to crystallization did not appear in DSC observation for the blends with a small amount of PE such as SE54/HPS-27, SE54/LPS-27, SE73/HPS-26 and SE73/LPS-26. This means that the crystallization of PE chains is confined to the microdomain and that in particular crystallization is much restricted in the rigid spherical and cylindrical domains.

3.1.2. Blends with PE homopolymer

Fig. 2 shows the SAXS profiles for the blends of SE with PE homopolymer in the molten state at 140 °C and the state crystallized isothermally at 74 °C.

In the molten state of SE34/LPE-58 containing 36% of LPE, morphology is changed from cylindrical to lamellar and the position of the first-order peak shifts to a low angle side compared to that of neat SE34. In SE34/LPE-67 which contains 50% of LPE, although the first-order peak position is hidden by the beam stopper, the SAXS profile is similar to that for SE34/LPE-58. For both blends of SE34/LPE-67 and /LPE-58, only one set of scattering peaks appears but any other series of peaks is not observed, and two exothermal peaks due to crystallization were not observed in the DSC measurements, contrastive to SE34/HPE-58 mentioned later. This suggests that LPE homopolymer is dissolved in the PE domain of the block copolymer because the molecular weight

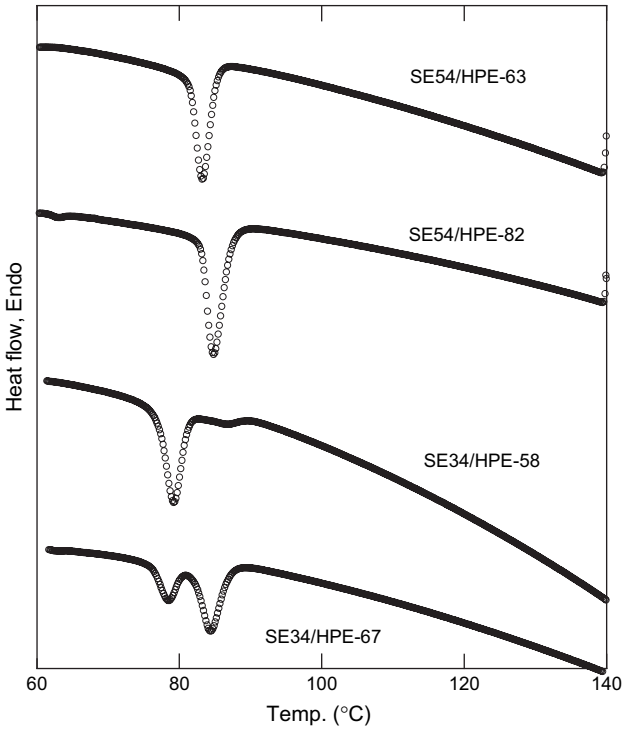

Fig. 3. DSC thermograms during non-isothermal crystallization process for SE34/HPE and SE54/HPE.

of LPE is smaller than that of PE block in SE34. On the other hand, the blends with HPE whose molecular weight is much higher than that of PE block in SE34 macrophase-separate, as shown clearly for SE34/HPE-58 in Fig. 2. Two series of peaks exist for SE34/HPE-58. This means that the system separates into two kinds of macrophases, in which one of them has lamellar structure and the other one probably cylindrical structure taking account of the SAXS profile in SE34/HPE-67. Also, the positions of the first-order peaks of both series exist at a lower angular position than that of neat SE, namely HPE homopolymers are distributed to both macrophases. For SE34/HPE-67 containing more amount of HPE, only one series of peaks due to cylindrical microphase structure is observed. However, the first-order peak position is almost the same as that of SE34/HPE-58 with a smaller amount of HPE, and in addition, as shown in Fig. 3, two exothermal peaks appear in crystallization in the same way as SE34/HPE-58. Therefore, it is concluded that SE34/HPE-67 also has two macrophases with cylindrically microphase-separated and disordered phases, respectively.

In the molten state of SE54 blends, although peak positions are not clearly observed, the SAXS profiles suggest an existence of lamellar microphase structure for SE54/LPE-63 and SE54/HPE-63 containing 20% of PE homopolymer, while SE54/

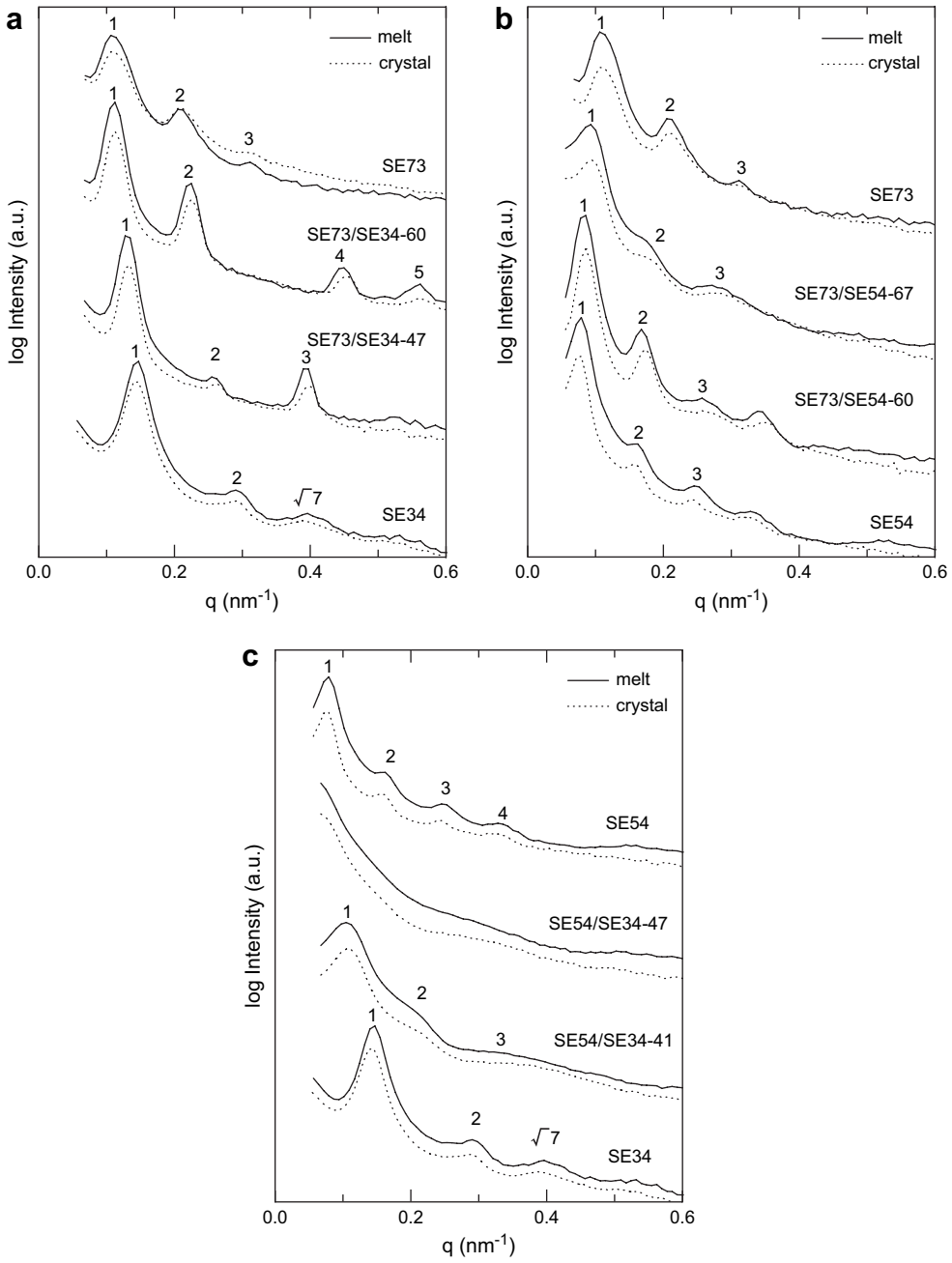

Fig. 4. SAXS profiles for SE and SE/SE in the molten state at 140 °C and the crystalline state at 74 °C.

LPE-82 and SE54/HPE-82 with 60% of PE homopolymer may be in the disordered state or not so regularly ordered state.

In the crystalline state of all SE34 and SE54 blends with PE, a broad peak due to crystalline lamellae can be observed at $q = 0.2-0.5$ in the same way as that for LPE and HPE homopolymers, while such a peak is not observed in the neat block copolymers. The broad peak suggests that the domain size in the blends was enlarged so that a few crystalline lamellae were able to be piled up within the domain. For SE34/LPE-58, as an example, the estimated PE domain size and the spacing between crystalline lamellae, are 52 nm and around 18 nm (for $q = 0.35\ \mathrm{nm}^{-1}$), respectively. Taking account of distribution of crystalline lamellar size, it is possible that a few crystalline lamellae are piled up in the PE domain between PS phases. Here, the "spacing between crystalline lamellae" is not necessarily a so-called long period because the orientation of chain-folded crystals within the microdomain is unknown but may be distributed in the present block copolymers. Zhu et al. [23] observed that the average chain orientation within the restricted rigid domain depended on T_c, and Hamely et al. [24] reported that it tended to be parallel to the domain surface in high molecular weight blocks to match the interfacial area per block junction between the crystalline and amorphous domains (The chain length scale is $\sim N^{2/3}$ for a block copolymer melt and $\sim N$ for a crystalline stem, where N is the degree of polymerization.). In addition, the chain direction may be confined so that the spacing of the microphase structure can be maintained in crystallization.

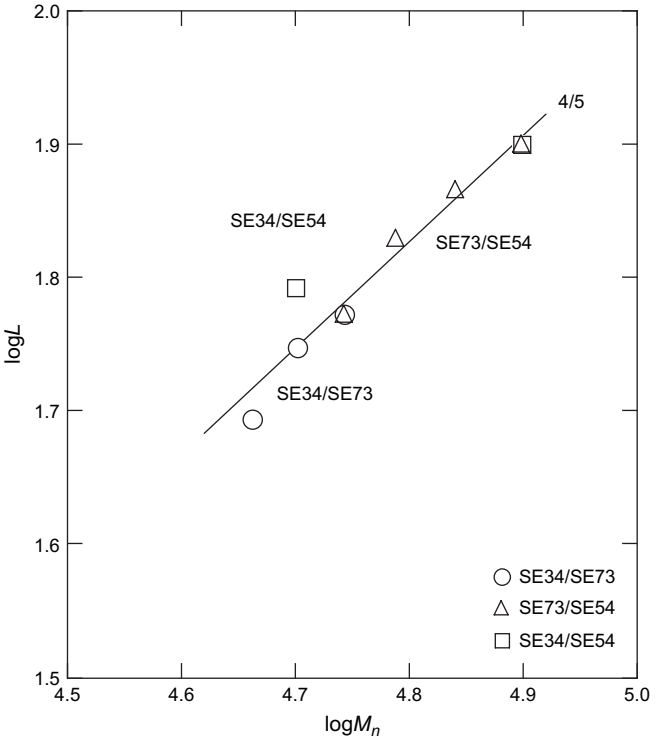

Fig. 5. Double logarithm plots of spacing L vs. number averaged molecular weight M_n for the SE/SE blends.

3.1.3. SE/SE blends

The SAXS profiles for the copolymer/copolymer blends are shown in Fig. 4. In the amorphous state, all samples except SE54/SE34-47 show clear peaks including higher-order peaks, which suggests that no macrophase separation occurs. The morphology of the blends with SE34 is changed from cylindrical to lamellar by adding SE73 or SE54. The position of the first-order peak in the lamellar structure depends on the blend composition for all blends. The spacing L and the domain size d are listed in Table 2. Fig. 5 shows double logarithm plots of spacing vs. number averaged molecular weight for the blends with lamellar structure. The slope of the plots is about 4/5. Hashimoto reported that the slope was in the range of 2/3–4/5 [25].

In the crystalline state, the peak positions are completely the same as those in the molten state. This means that the microphase separation structure in the melt was not disrupted by crystallization.

3.2. Crystallization behavior

Degrees of crystallinity, D.C., normalized to PE content, at various crystallization temperatures are summarized in Table 4 and are shown in Fig. 6.

As mentioned above, crystallization was not observed even at the condition of large supercooling degree ($T_c = 40\ ^\circ\mathrm{C}$) for both SE54/HPS-27 and SE54/LPS-27. The degree of crystallinity of neat SE34 is also very small. These are crystallization within the spherical or cylindrical microdomain surrounded by glassy PS. We reported previously the same behavior for poly(tetrahydrofuran)–PS block copolymers, and concluded that it was very hard to crystallize within a closed *rigid* microdomain [26]. On the other hand, SE54/HPS-43 and SE54/LPS-43 have a D.C. of 20–25% as shown in Table 4. In these two blends, their melt morphology is lamellar as shown in Fig. 1a and b.

SE34/HPE-58 and SE34/HPE-67 show two exothermal peaks in non-isothermal crystallization as seen in the DSC curves of Fig. 3, which corresponds to macrophase separation occurring (Fig. 2a) as mentioned already. For comparison, the thermograms for SE54/HPE-63 and SE54/HPE-82 without macrophase separation in the melt are also shown in Fig. 3. In both SE34/HPE-58 and SE34/HPE-67, the double crystallization peaks at a lower and higher temperatures can be assigned to the crystallizations from two macrophase-separated phases of cylindrical and lamellar (or disordered) ones, respectively, because the crystallization from the former phase is more restricted than that from the latter. In fact, the peak position at a higher temperature is close to that for SE54/HPE-63 and SE54/HPE-82 crystallized from the disordered or not so regularly ordered state as described above. Also, the area ratio of the double peaks is parallel to the content of PE homopolymer in the blends. Thus, the peaks at the lower and higher temperatures correspond to crystallization from the cylindrical domain and from the lamellar domain (or disordered state), respectively.

Table 4
Melting temperature, degree of crystallinity and Avrami index in the indicated range of T_c

Sample	T_c (°C)	$T_{m\ low}$ (°C)	$T_{m\ high}$ (°C)	D.C.[a] (%)	Avrami index
SE34	71.9–75.0	84.2–89.3	94.0–95.2	5.3–3.3	1.5–1.8
SE54	83.0–85.0	87.4–89.2	96.1–96.4	28.3–26.0	2.2–2.3
HPE	90.2–93.2	93.1–96.4	99.4–100.8	26.8–22.8	2.6–3.1
LPE	103.0–106.0	108.8–110.7	111.0–112.9	31.5–18.7	2.4–3.1
SE54/HPS-43	82.0–84.0	86.6–87.7	97.1–97.5	23.4–22.4	1.8–1.9
SE54/HPS-27[b]	40	–	–	–	–
SE54/LPS-43	84.0–86.0	88.9–90.6	98.6–98.8	25.5–21.4	2.5–2.6
SE54/LPS-27[b]	40.0	–	–	–	–
SE34/LPE-58	102.0–104.0	104.2–106.3	110.0–111.2	17.9–12.6	2.4–2.5
SE34/LPE-67	102.0–104.0	103.4–106.5	110.2–111.2	21.2–15.1	2.0
SE54/LPE-63	95.0–97.0	98.5–100.5	106.9–107.5	22.7–16.6	2.0
SE54/LPE-82	104.0–106.0	106.9–108.8	109.2–110.2	14.3–8.7	2.0–2.3
SE54/HPE-63	86.0–89.0	90.3–93.1	97.5–98.4	22.5–18.0	2.4–2.7
SE54/HPE-82	88.0–91.0	91.5–94.4	98.1–98.9	25.1–21.0	2.1–2.6
SE54/SE34-41	79.0–82.0	83.8–87.4	95.1	24.6–22.8	2.0–2.7
SE54/SE34-47	81.0–83.0	86.3–88.1	95.1–95.5	29.1–25.5	2.2–2.7

[a] Normalized to PE content. $\Delta H_m^o = 4.051$ kJ/mol was used [30].
[b] Crystallization was not observed.

For all crystallizable samples, as examples are shown in the DSC curves of Fig. 7, two endothermal peaks appeared in the melting process after crystallized isothermally, in spite of a single exothermal peak in the crystallization except for the above two macrophase-separated samples. A lower melting peak depended on T_c, whereas a higher one was almost independent of T_c. This means that the former melting peak is due to crystals formed by isothermal crystallization at the T_c and that the latter is due to reorganization of crystals during the DSC scan. These two kinds of melting temperatures are plotted against T_c in Fig. 8. The plots of lower melting temperature $T_{m\ low}$ vs. T_c are parallel to $T_m = T_c$, so that common Hofman–Weeks plots cannot be used to decide the equilibrium melting temperature T_m^o. This melting behavior including multimodal endotherms has been found and discussed so far for hydrogenated PBd and ethylene random copolymers such as linear low density polyethylene (LLDPE) and ethylene–vinyl acetate copolymers [27–29]. Therefore, the behavior that the $T_{m\ low}$ vs. T_c plots are parallel to $T_m = T_c$ is not peculiar to block copolymer itself. This may come from distribution of melting temperatures originating from distribution of ethyl-branch

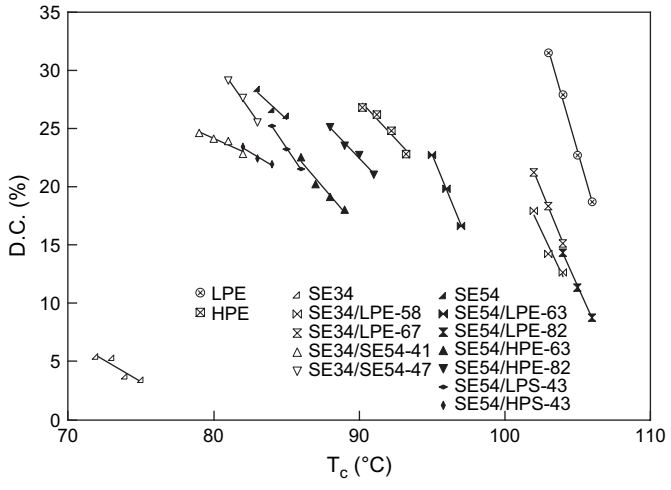

Fig. 6. Plots of degrees of crystallinity, D.C., vs. crystallization temperature T_c for indicated samples.

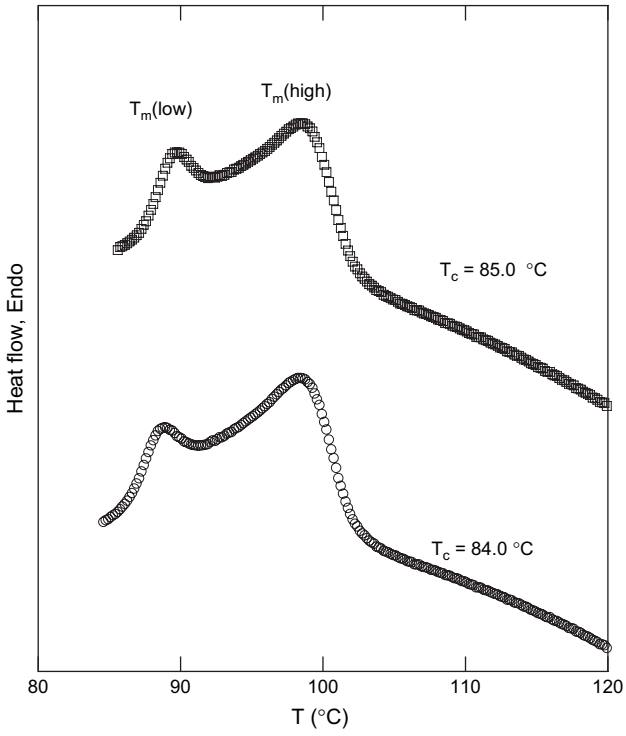

Fig. 7. DSC thermograms in the melting of SE54/LPS-43 crystallized at the indicated temperature.

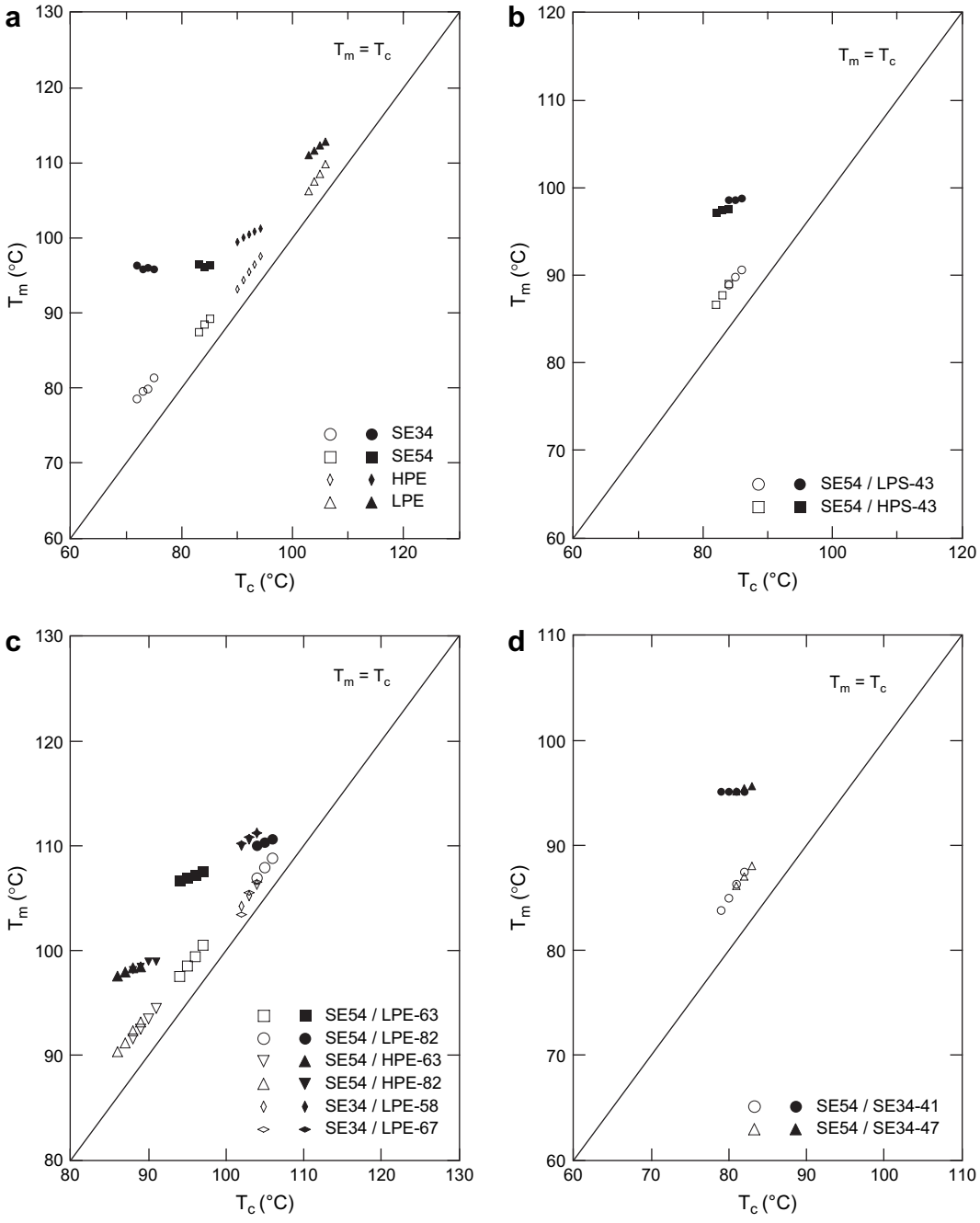

Fig. 8. Hoffman–Weeks plots. For each sample $T_{m\ high}$ is indicated with filled symbols and $T_{m\ low}$ with open symbols.

composition. When the melting temperatures of the samples are distributed in the region crossing over a given crystallization temperature T_c, the plots of T_m vs. T_c may be parallel to $T_m = T_c$ because the polymers with T_m lower than T_c cannot crystallize. Then, D.C. should decrease with T_c, because the number of the polymers with T_m above T_c decreases with increasing crystallization temperature. It was observed that T_m, T_c and D.C. decreased with increasing amount of branches for the fractionated LLDPE [28,29].

For both SE54 blends with HPS and LPS, as shown in Fig. 6, although D.C. is reduced by adding PS homopolymers, the plots of D.C. are located in the T_c–D.C. region close to that of neat SE54, because in this case all PE components belong to the block copolymer and the melt morphology of the blends is the same as neat SE54. On the other hand, the SE54 blends are affected by blending PE homopolymer. The behavior of D.C. for the blends with HPE and LPE comes close to that for HPE and LPE, respectively, depending on the amount of added PE (the fractions of HPE and LPE homopolymers in the whole PE component are 0.32 and 0.74 for SE54/PE-63 and SE54/PE-82, respectively). This suggests that PE chains in the homopolymer and copolymer crystallize

together. On the other hand, D.C. behavior in the SE34 blends is much governed by PE homopolymer (the fraction of LPE in the whole PE: 0.62 and 0.75 for SE34/LPE-58 and SE34/LPE-67, respectively). This may be due to the following blending effects: morphology change from cylindrical to lamellar, enlargement of the domain size, and disordering of morphology, as shown in Fig. 2b.

The feature in the crystallization kinetics of the polymer systems including block copolymers has been discussed mainly on the basis of Avrami expression. According to Avrami equation, the fraction of crystallinity X_t at a crystallization time t is expressed as

$$X_t = 1 - \exp(-Kt^n) \tag{4}$$

where K is the overall crystallization rate constant and n is the Avrami index. Since Eq. (4) can be rewritten as

$$\log[-\ln(1 - X_t)] = \log K + n\log t \tag{5}$$

n can be evaluated from the initial slope of the plots of $\log[-\ln(1 - X_t)]$ vs. $\log t$. At a small degree of crystallinity, Eq. (5) can be rewritten as

$$\log X_t = \log K + n\log t \tag{6}$$

Fig. 9 shows an example of double logarithm plots of X_t against t. The Avrami indices n obtained from the initial slope of the plots are summarized in Table 4. As shown in Table 4, Avrami indices of the block copolymers and blends are smaller than those of PE homopolymers. In particular, n of SE34 with a cylindrical domain is very small, and that of SE54/HPS-43 is also small. The small value of n, which means the decrement of the growth dimension, is caused by a restriction in crystallization within the microphase-separated domain, in particular, within two- or three-dimensionally closed domains such as cylindrical and spherical domains.

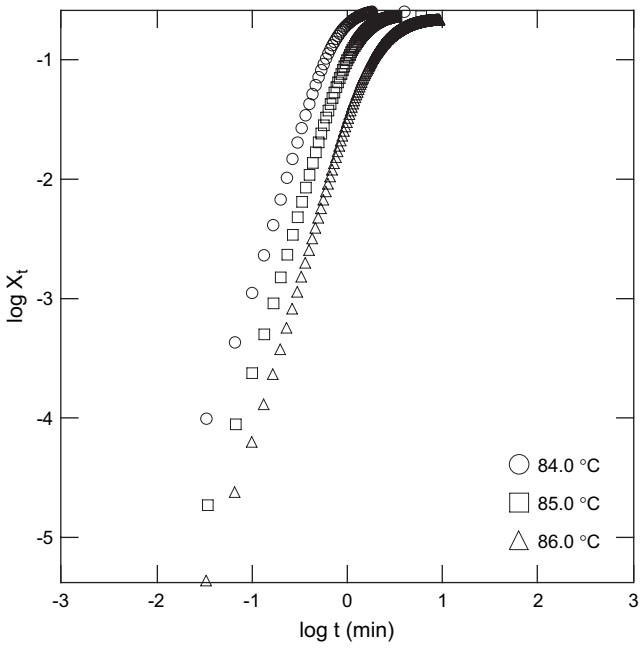

Fig. 9. Avrami plots for SE54/LPS-43 at indicated T_c.

The inverse of the crystallization time τ at a certain degree of crystallinity X_τ corresponds to the overall crystallization rate v, that is,

$$v \sim 1/\tau \tag{7}$$

Here, τ was taken to be the time at $X_\tau = 0.015$, which lies on the straight line of the $\log t - \log X_\tau$ relation for all the samples. Fig. 10 shows Arrhenius-type plots of $1/\tau$, that is, $1/t_{0.015}$ vs. the inverse of the supercooling degree $\Delta T = T_m^o - T_c$, where the equilibrium melting temperature T_m^o was assumed to be 145 °C [30] which is for the linear PE homopolymer.

As seen in Fig. 10a, the slope of the plots, that corresponds to the apparent activation energy of crystallization, is steep for SE54/HPS-43 compared with that of neat SE54. This tendency can be attributed to the fact that the increasing glassy component PS restricts the crystallization of blends.

As shown in Fig. 10b–d, the crystallization rate of SE block copolymers is much slower than that of PE homopolymers when compared with each other at the same ΔT, and the apparent activation energy of SE is larger. When adding homopolymer PE to SE, both crystallization rate and activation energy come close to those of PE homopolymer depending on the amount of added PE. This tendency of the composition dependence coincides to that in the behavior of D.C. For the block copolymer/block copolymer blend SE54/SE34, as shown in Fig. 10e, the Arrhenius-type plots shift depending on the blend ratio.

4. Conclusion

The macrophase separation and the morphological change in microphase separation occurred depending on both blend composition and molecular weight of added homopolymer for the SE blends with the corresponding homopolymer and for the SE/SE blends, as reported so far for the blends containing block copolymers.

In crystallization, the melt structure was completely maintained for all blends, irrespective of the microphase separation structure and with and without macrophase separation, because the structure is *frozen* by the glassy PS. This suggests that the crystalline phase can be arranged in the several-ten nanometer scale by applying the melt structure as a template.

The crystallization of SE/PS was restricted with an increase of glassy PS component with both aspects of the crystallinity and crystallization kinetics, and at last the crystallization was not observed for the SE/PS blends with spherical PE domains. On the other hand, the crystallization of SE/PE was not restricted so much to come close to the crystallization behavior in PE homopolymer with increasing PE content. In the macrophase-separated systems the crystallization occurred independently in the respective phases, while in the other systems the exothermal crystallization peak was single.

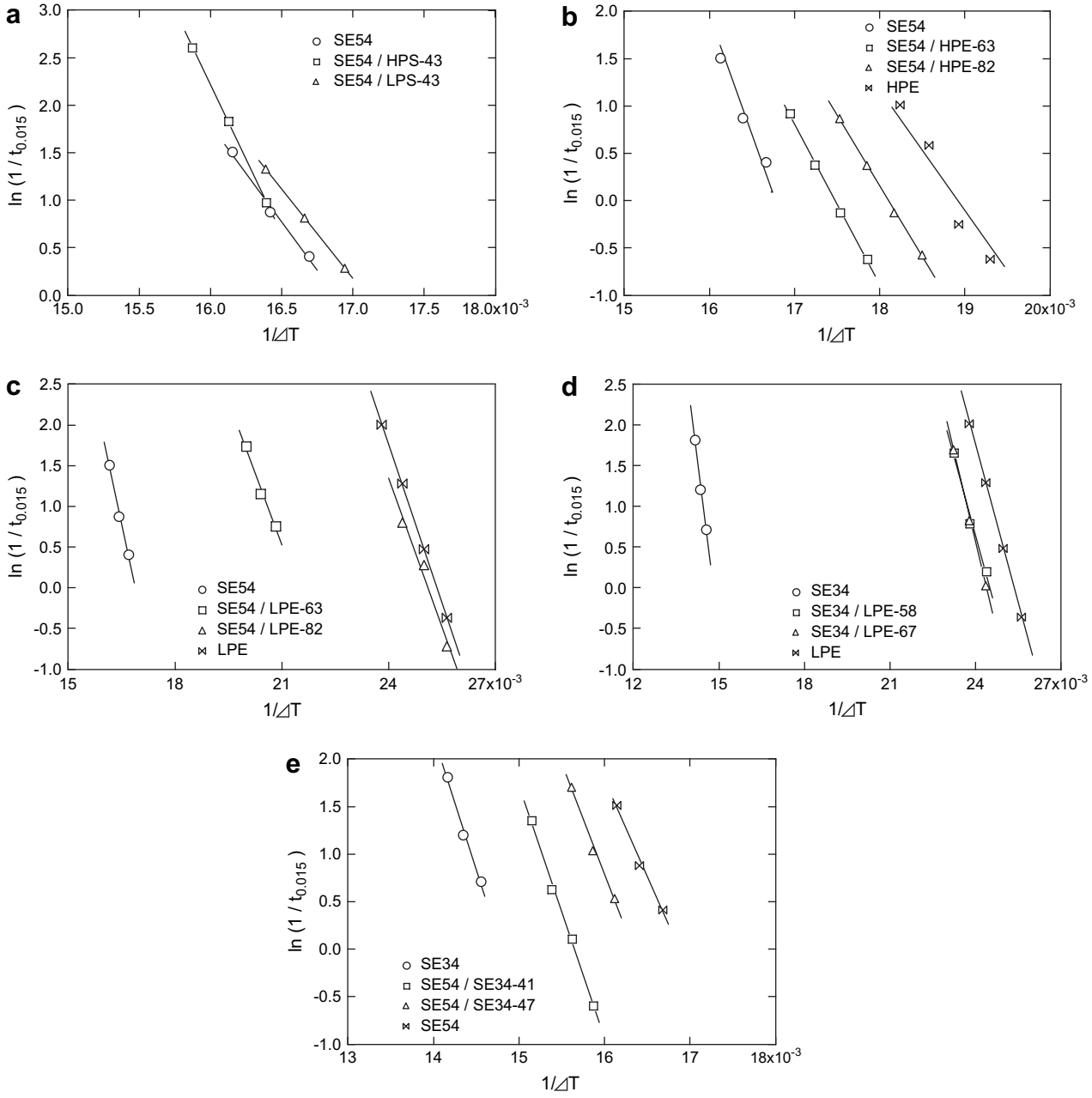

Fig. 10. Arrhenius-type plots of the overall crystallization rate vs. the reciprocal of the supercooling degree for indicated samples.

Acknowledgements

This work was supported by Grants-in-Aid for Exploratory Research (18655092) from Japan Society for the Promotion of Science and by the 21st Century COE Program for Scientific Research from the Ministry of Education, Culture, Sports, Science and Technology. This work was performed under the approval of the Photon Factory Program Advisory Committee (Proposal Nos. 2004G087 and 2004G338).

References

[1] Hamley IW. The physics of block copolymer. New York: Oxford; 1998 [chapter 5].
[2] Chen HL, Wu JC, Lin TL, Lin JS. Macromolecules 2001;34:6936–44.
[3] Nojima S, Kato K, Yamamoto S, Ashida T. Macromolecules 1992;25: 2237–42.
[4] Quiram DJ, Marchand GY, Register RA. Macromolecules 1997;30: 4551–8.
[5] Loo YL, Ryan AJ, Register RA. Macromolecules 2002;35:2365–74.
[6] Ryan AJ, Hamley IW, Bras W, Bates FS. Macromolecules 1995;28: 3860–8.
[7] Ho RM, Chung TM, Tsai JC, Kuo JC, Hsiao B, Sics I. Macromol Rapid Commun 2005;26:107–11.
[8] Quiram DJ, Register RA, Ryan AJ. Macromolecules 1997;30:8338–43.
[9] Zhu L, Mimnaugh BR, Cheng SZD. Polymer 2001;42:9121–31.
[10] Ho RM, Lin FH, Tsai CC, Sics I. Macromolecules 2004;37:5985–94.
[11] Sakurai K, MacKnight WJ, Lohse DJ, Schulz DN, Sissano JA. Macromolecules 1993;26:3236–8.
[12] Hsu JY, Nandan B, Chen MC, Chiu FC, Chen HL. Polymer 2005;46: 11837–43.

[13] Talibuddin S, Wu L, Runt J, Lin JS. Macromolecules 1996;29:7527–35.
[14] Sakurai K, MacKnight WJ, Lohse DJ, Schulz DN, Sissano JA. Macromolecules 1994;27:4941–51.
[15] Huang P, Zhu L, Guo Y, Chen WY, Sics I. Macromolecules 2004;37:3689–98.
[16] Shiomi T, Takeshita H, Kawaguchi H, Nagai M, Takenaka K, Miya M. Macromolecules 2002;35:8056–65.
[17] Huang YY, Yang CH, Liou W. Macromolecules 2004;37:486–93.
[18] Takeshita H, Ishii N, Araki C, Shiomi T. J Polym Sci Part B 2004;42:4199–206.
[19] Ueki T, Hiiragi Y, Kataoka M, Inoko Y, Amemiya Y, Izumi Y, et al. Biophys Chem 1985;23:115–24.
[20] Olabisi O, Simha R. Macromolecules 1975;8:206–10.
[21] Höcker H, Blake GJ, Flory PJ. Trans Faraday Soc 1971;67:2251–7.
[22] Hashimoto T, Tanaka H, Hasegawa H. Macromolecules 1990;23:4378–86.
[23] Zhu L, Cheng ZD, Calhoun BH, Ge Q, Quirk RP, Thomas EL, et al. J Am Chem Soc 2000;122:5957–67.
[24] Hamely IW, Fairclough JPA, Terrill NJ, Ryan AJ, Lipic PM, Bates FS, et al. Macromolecules 1996;29:8835–43.
[25] Hashimoto T. Macromolecules 1982;15:1548–53.
[26] Shiomi T, Tsukada H, Takeshita H, Takenaka K, Tezuka Y. Polymer 2001;42:4997–5004.
[27] Alamo RG, Chan EKM, Mandelkern L, Voigt-Martin IG. Macromolecules 1992;23:6381–94.
[28] Vandermiers C, Moulin J-F, Damman P, Desiere M. Polymer 2000;41:2915–23.
[29] Mirabella FM. J Polym Sci Part B 2001;39:2800–18.
[30] Brandrup J, Immergut EH. Polymer handbook. 3rd ed. Wiley Interscience; 1989 [part V].